Article

Molecular Acrobatics: Self-Assembly of Calixarene-Porphyrin Cages

Laura Baldini, Pablo Ballester, Alessandro Casnati, Rosa M. Gomila, Christopher A. Hunter, Francesco Sansone, and Rocco Ungaro

J. Am. Chem. Soc., **2003**, 125 (46), 14181-14189• DOI: 10.1021/ja036758a • Publication Date (Web): 24 October 2003

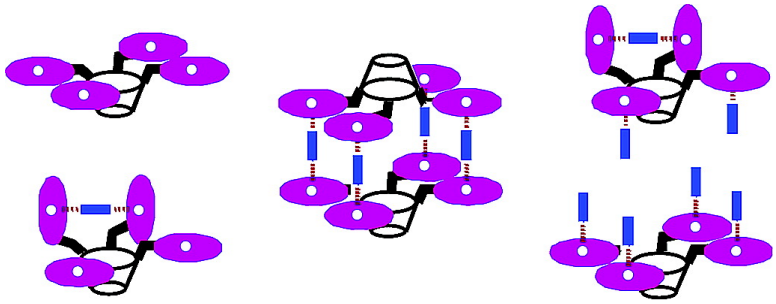

J|A|C|S
ARTICLES
Published on Web 10/24/2003

Molecular Acrobatics: Self-Assembly of Calixarene-Porphyrin Cages

Laura Baldini,[†] Pablo Ballester,[§] Alessandro Casnati,[†] Rosa M. Gomila,[§] Christopher A. Hunter,*[,‡] Francesco Sansone,[†] and Rocco Ungaro[†]

Contribution from the Dipartimento di Chimica Organica e Industriale, Universita' di Parma, Italy, Centre for Chemical Biology, Krebs Institute for Biomolecular Science, Department of Chemistry, University of Sheffield, Sheffield S3 7HF, UK, and Departament de Química, Universitat de les Illes Balears, 07122 Palma de Mallorca, Illes Balears, Spain

Received June 18, 2003; E-mail: c.hunter@shef.ac.uk

Abstract: Calix[4]arenes equipped with two and four zinc porphyrins have been prepared, and they show remarkable flexibility in their self-assembly properties with the bidentate ligand DABCO. The calix-bisporphyrin forms a 2:2 complex with DABCO, generating a large cavity that has the potential to act as a supramolecular host. The calix-tetraporphyrin, on the other hand, forms four different complexes with DABCO depending on the stoichiometry and concentration. During the course of a titration, all four complexes are populated, leading to large conformational changes and the formation of both intramolecular and intermolecular calix-tetraporphyrin−DABCO sandwich complexes. The system was fully characterized using a combination of UV−visible and ^{1}H NMR spectroscopy to identify the complexes. At a calix-tetraporphyrin: DABCO ratio of 2:4, the major species is dimeric cage assembly that features a large internal cavity for guest complexation.

Introduction

The formation of cage-like macromolecular structures is of great interest due to the ability of the enclosed cavity to encapsulate a substrate. Once surrounded by the receptor, the guest occupies a confined space that provides protection from the external medium, mediates transport between phases, or constitutes a nanoscale reaction chamber.[1] To facilitate the synthesis of large and well-defined molecular architectures and to promote reversible encapsulation, self-assembly has proved to be a useful and versatile technique.[2] Noncovalent interactions such as hydrogen bonding or metal−ligand interactions are significantly weaker than covalent bonds, but the presence of many weak interactions can provide a sufficient thermodynamic driving force to assemble relatively stable cage complexes.[3] Preorganization of the subunits is highly desirable to minimize the entropy losses due to intermolecular association and to the freezing of rotational degrees of freedom during the ring-closure process.[4] Complex, well-defined supramolecular arrays can thus be constructed in a single step simply upon mixing, under the appropriate conditions, judiciously chosen components.

Subunits with a hemispherical structure are particularly attractive, because face-to-face dimerization results in a supramolecular assembly possessing a defined, almost spherical cavity.[5] Calixarenes locked in the cone conformation and resorcinarenes have been widely exploited in recent years as building blocks for the self-assembly of capsule-like structures.[6] These macrocycles have a well-defined hydrophobic cavity, and the rims can be easily functionalized. The introduction of urea groups in the upper rim enabled Rebek,[7] de Mendoza, and Pochini[8] to construct several self-complementary calix[4]- and calix[6]arenes that dimerize in apolar solvents through hydrogen

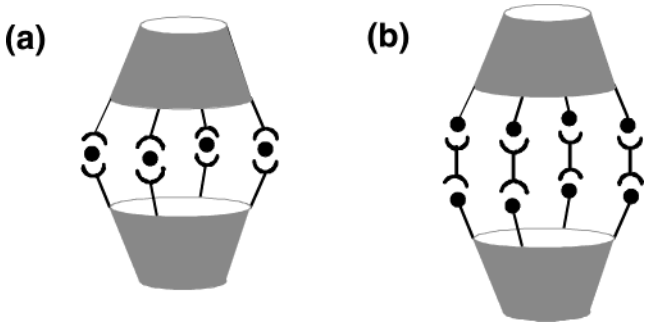

Figure 1. Dalcanale's resorcinarene dimer is assembled via coordination of four metals (●). (b) The strategy employed here is assembly of a calixarene bearing four metal centers (●) via coordination of four bidentate ligands.

[†] Universita' di Parma.
[‡] University of Sheffield.
[§] Universitat de les Illes Balears.

(1) Jasat, A.; Sherman, J. C. *Chem. Rev.* **1999**, *99*, 931−967.
(2) Conn, M. M.; Rebek, J. *Chem. Rev.* **1997**, *97*, 1647−1668.
(3) Philp, D.; Stoddart, J. F. *Angew. Chem., Int. Ed. Engl.* **1996**, *35*, 1155−1196.
(4) Rebek, J. *Acc. Chem. Res.* **1999**, *32*, 278−286.
(5) MacGillivray, L. R.; Atwood, J. L. *Angew. Chem., Int. Ed.* **1999**, *38*, 1019−1034.
(6) Rudkevich, D. M. Self-assembly in solution. In *Calixarenes 2001*; Asfari, Z., Bohmer, V., Harrowfield, J., Vicens, J., Eds.; Kluwer Academic Publishers: Norwell, MA, 2001; pp 155−180.
(7) Shimizu, K. D.; Rebek, J. *Proc. Natl. Acad. Sci. U.S.A.* **1995**, *92*, 12403−12407.
(8) Gonzalez, J. J.; Ferdani, R.; Albertini, E.; Blasco, J. M.; Arduini, A.; Pochini, A.; Prados, P.; de Mendoza, J. *Chem.-Eur. J.* **2000**, *6*, 73−80.

10.1021/ja036758a CCC: $25.00

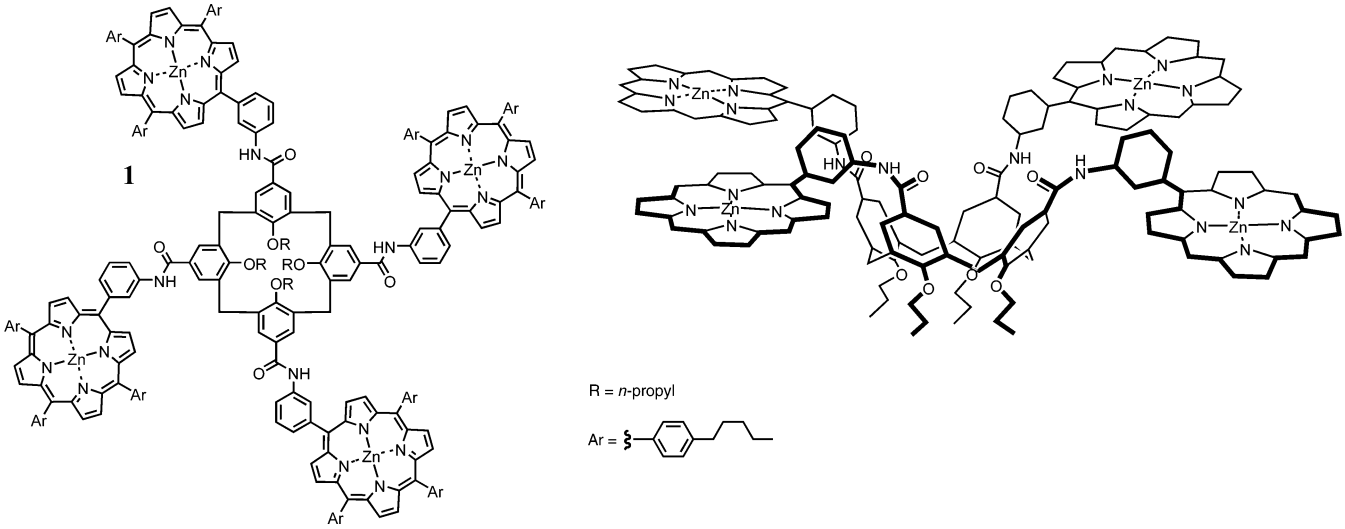

Figure 2. Structure of the calix-tetraporphyrin **1**, and a view of one possible conformation (side chains and double bonds omitted for clarity).

bonding. Small organic molecules were shown to fit into the capsule and sometimes even to template its formation.[9]

Metal−ligand interactions have been exploited to obtain self-assembling capsules based on calixarenes and resorcinarenes.[6] In 1994, Shinkai introduced two acetylacetonate groups on the upper rim of a calix[4]arene and showed that it formed a dimeric capsule upon chelation to two Cu^{2+} cations.[10] Dalcanale functionalized a resorcinarene with four donor groups in the correct orientation to promote dimerization upon coordination to four metals (Figure 1a).[11] In the 2:4 complex, the two square pyramidal moieties of the calixarene face each other in an approximately octahedral overall geometry. We describe here a new approach to the self-assembly of a supramolecular calix[4]arene capsule through metal−ligand interactions. In this case, tetrafunctionalization of the calixarene upper rim with metal complexes gives subunits that dimerize in a face-to-face fashion upon addition of an appropriate bidentate ligand (Figure 1b). This approach reverses the metal−ligand relationships employed until now in the self-assembly of calix- and resorcinarenes.

The introduction of the metal centers on the calixarene scaffold was accomplished by functionalization of the calixarene upper rim with metalloporphyrins. We chose porphyrins because they are rigid, they can easily be functionalized, and a number of different metals can be inserted in the center of the macrocycle. The central metal of the porphyrin is coordinated to four nitrogens and can accept either one or two additional apical donor atoms to give a square pyramidal or octahedral coordination sphere, respectively. Zinc porphyrins are five-coordinate, so only one interaction with a bidentate ligand is possible, and this can lead to self-assembly of higher order structures. Molecular models suggested that compound **1** (Figure 2) can assume a conformation that places all of the porphyrin units in approximately the same plane, promoting self-assembly of the 2:4 complex shown in Figure 1b in the presence of a linear bidentate ligand. The calixarene is locked in the cone conformation by the four propyl groups on the lower rim, the amide linkers are relatively rigid, and the porphyrins are spaced far apart to reduce competition from intramolecular interactions.

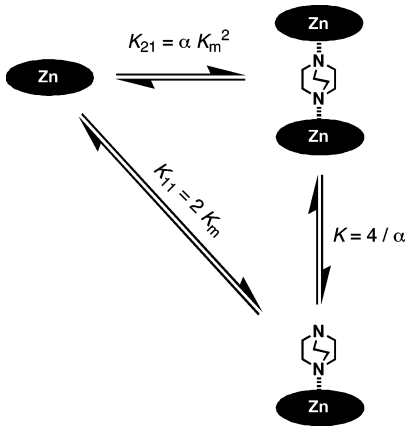

Figure 3. Simple zinc porphyrins form 1:1 complexes with DABCO at low porphyrin concentrations (micromolar). At higher concentrations (millimolar), 2:1 sandwich complexes are formed in the presence of excess porphyrin. K_m is the microscopic association constant for the interaction of one DABCO nitrogen with a zinc porphyrin. α is the cooperativity factor that quantifies how binding one DABCO nitrogen affects the binding interaction at the second DABCO nitrogen. Stepwise equilibrium constants (K), overall stability constants (K_{11} and K_{21}), and statistical correction factors for the equilibria are also shown.

This paper describes the synthesis and self-assembly properties of **1** and of the analogous calix-bisporphyrin **9** in the presence of 1,4-diazabicyclo[2.2.2]octane (DABCO). The zinc porphyrin−DABCO system has been widely studied by Sanders and Anderson.[12−15] For simple zinc porphyrins at micromolar concentrations, a 1:1 complex is formed with an association constant of about 10^5 M^{-1} in organic solvents (Figure 3). At millimolar concentrations, when 0.5 equiv of DABCO is added, the 2:1 porphyrin−DABCO sandwich complex is formed, but this opens up to give the 1:1 complex in the presence of excess DABCO (Figure 3). Zinc porphyrin oligomers can be assembled into more complex architectures such as ladders based on the 2:1 porphyrin−DABCO sandwich motif,[14,15] and this is the

(9) Rebek, J. *Chem. Commun.* **2000**, 637−643.
(10) Fujimoto, K.; Shinkai, S. *Tetrahedron Lett.* **1994**, *35*, 2915−2918.
(11) Jacopozzi, P.; Dalcanale, E. *Angew. Chem., Int. Ed. Engl.* **1997**, *36*, 613−615.
(12) Hunter, C. A.; Meah, M. N.; Sanders, J. K. M. *J. Am. Chem. Soc.* **1990**, *112*, 5773−5780.
(13) Anderson, H. L.; Hunter, C. A.; Meah, M. N.; Sanders, J. K. M. *J. Am. Chem. Soc.* **1990**, *112*, 5780−5789.
(14) Anderson, H. L. *Inorg. Chem.* **1994**, *33*, 972−981.
(15) Taylor, P. N.; Anderson, H. L. *J. Am. Chem. Soc.* **1999**, *121*, 11538−11545.

Scheme 1

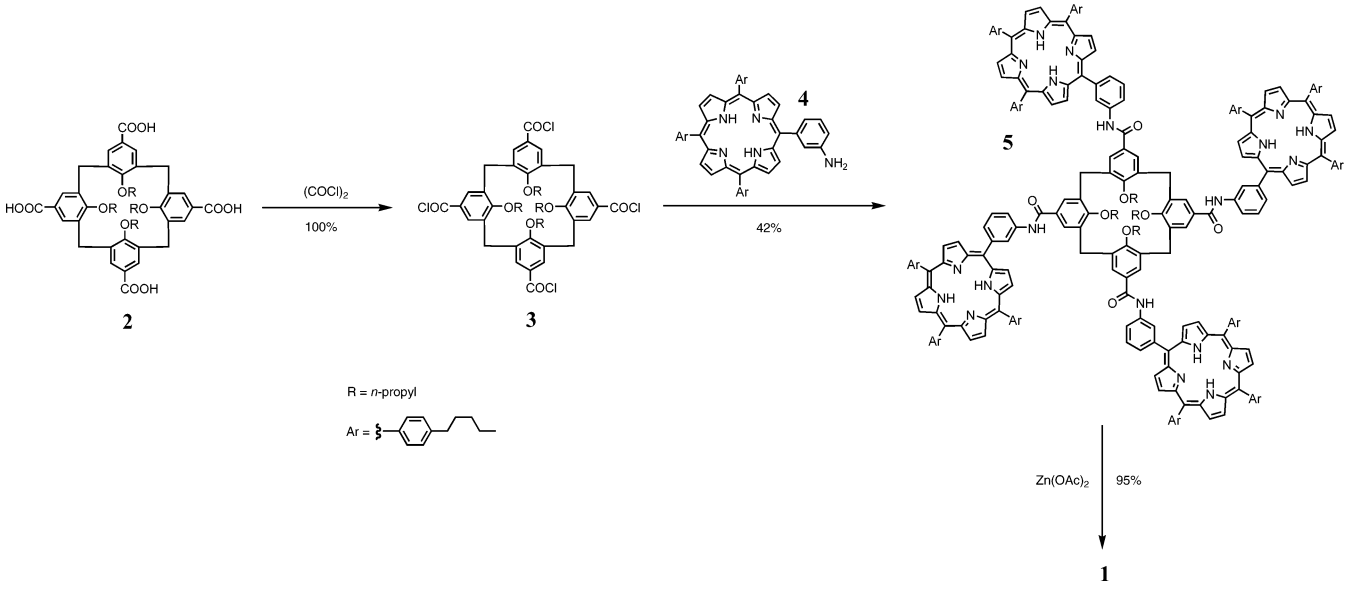

Scheme 2

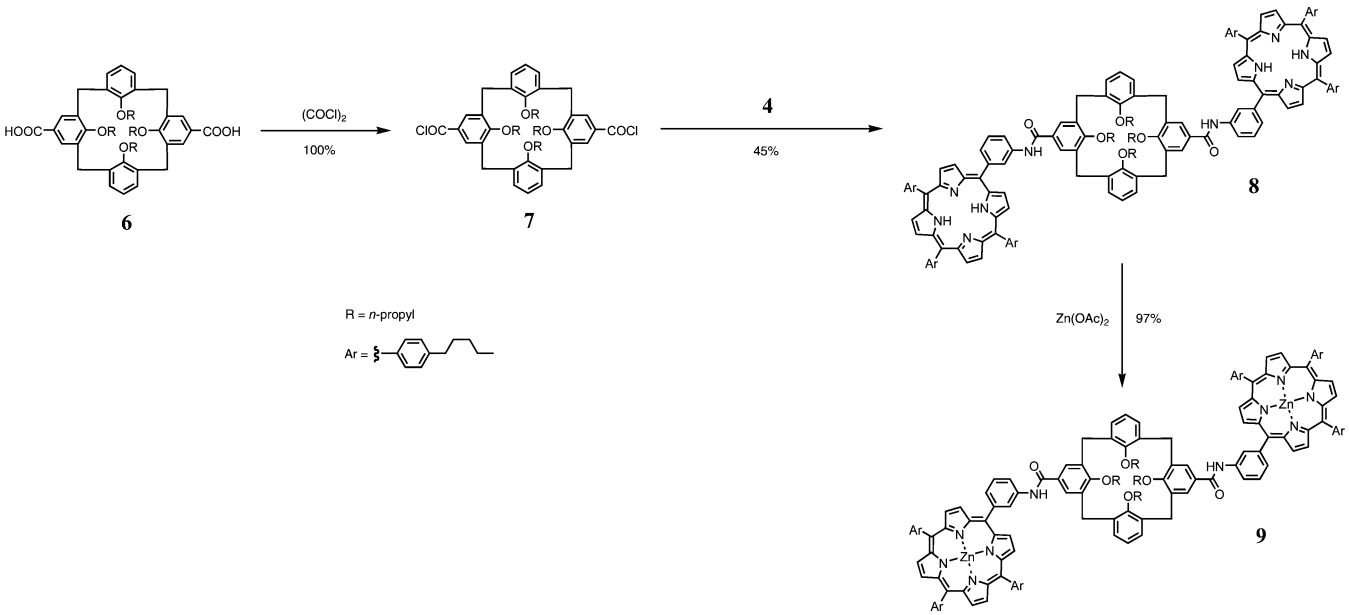

system exploited here for the construction of a supramolecular cage.

Results and Discussion

The calix-bisporphyrin **9**, having only two zinc porphyrins in the diametral (1,3) positions of the calixarene upper rim, was prepared as a simpler model system, and the study of its behavior in the presence of DABCO was essential for clarifying some mechanistic features of the **1**−DABCO interaction.

Synthesis. Tetrapropoxycalix[4]arene tetracarboxylic acid **2** was prepared according to a literature procedure starting from tetrapropoxycalix[4]arene.[16] Reaction of **2** with oxalyl chloride in refluxing dry CH_2Cl_2 gave tetrachloride **3** with no need for further purification (Scheme 1). Coupling with the amino porphyrin[17] **4** was accomplished by dropwise addition of a solution of **3** into a solution containing 12 equiv of the porphyrin in dry CH_2Cl_2. Column chromatography allowed the complete recovery of the unreacted porphyrin and the isolation of **5** in 42% yield. Metalation with zinc acetate furnished **1** in quantitative yield. The corresponding calix-bisporphyrin was synthesized starting from **6** by an analogous procedure to give **9** in 45% overall yield (Scheme 2).[16]

Conformational Properties. The ^{1}H NMR spectrum of the tetraporphyrin derivative **1** in $CDCl_3$ is almost concentration independent, and addition of d_5-pyridine does not significantly alter the spectrum. This indicates that there is no inter- or intramolecular aggregation as a consequence of porphyrin stacking interactions.[14] The ^{1}H NMR signals due to the protons of the calixarene are indicative of a tetrasubstituted calixarene derivative of C_{4v} symmetry. The aromatic region of the spectrum

(16) Sansone, F.; Barboso, S.; Casnati, A.; Fabbi, M.; Pochini, A.; Ugozzoli, F.; Ungaro, R. *Eur. J. Org. Chem.* **1998**, 897−905.

(17) Gardner, M.; Guerin, A. J.; Hunter, C. A.; Michelsen, U.; Rotger, C. *New J. Chem.* **1999**, *23*, 309−316.

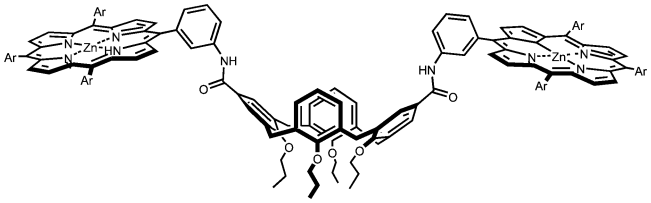

Figure 4. The flattened cone conformation of calix-bisporphyrin **9**.

is rather complicated, and COSY and ROESY experiments were required to fully assign all of the signals. This is due to slow rotation about the porphyrin *meso*-aryl bonds on the NMR time scale and the presence of the calixarene which makes the two faces of the porphyrin nonequivalent.[17] The bisporphyrin derivative **9** is in a pinched cone conformation with the aromatic rings bearing the porphyrins pointing outward (Figure 4), as is inferred from the upfield shift of the protons of the unsubstituted aromatic groups of the calixarene in the ^{1}H NMR spectrum.

Self-Assembly of Model Compounds. Before the self-assembly behavior of **1** and **9** in the presence of DABCO is discussed, it is useful to refer to simpler models to define some of the thermodynamic parameters that will be used in the interpretation of the results. The possible equilibria involved in the interaction of a simple monomeric zinc porphyrin with DABCO are shown in Figure 3. At micromolar concentrations of porphyrin, only the 1:1 complex is formed, and so UV−visible titrations of zinc tetra(4-*n*-pentylphenyl)porphyrin with DABCO were used to determine the value of K_m ($(8.9 \pm 0.5) \times 10^4$ M^{-1} in $CHCl_3$ and $(2.0 \pm 0.5) \times 10^5$ M^{-1} in CH_2Cl_2). When one DABCO nitrogen is bound to a zinc porphyrin, the affinity of the second nitrogen for another zinc porphyrin can be affected; that is, the two binding events are not independent. The cooperativity factor, α, is used to quantify this effect, and the value of α can readily be determined from ^{1}H NMR titrations. At millimolar concentrations of porphyrin, until 0.5 equiv of DABCO is added, only the 2:1 sandwich complex is formed, but this opens up to form the 1:1 complex with excess DABCO. The association constant for formation of the 2:1 complex is too large to be measured at these concentrations, but the equilibrium constant for breakdown of the sandwich complex ($K = 4/\alpha$) is weaker and can be measured. This experiment gave a value of $\alpha = 0.8 \pm 0.2$ in $CDCl_3$; that is, this effect is of minor significance in this system and will not be considered further.

Self-Assembly of the Calix-Bisporphyrin 9. Next, we will consider the self-assembly properties of the calix-bisporphyrin **9** in the presence of DABCO. The lower stoichiometry makes the analysis relatively simple as compared with **1**. We again studied this system using UV−visible and ^{1}H NMR titrations. The UV−visible titration data are shown in Figure 5. Upon addition of DABCO, the Soret band at 420 nm corresponding to the unbound zinc porphyrin gradually disappeared and a new band appeared at 425 nm. This new band is characteristic of a porphyrin−DABCO sandwich complex. As the concentration of DABCO increased, the 425 nm band decreased in intensity and a new band appeared at 430 nm. This band is characteristic of a simple porphyrin−DABCO complex.[12] Two clear isosbestic points are observed, and this is indicative of two sequential two-state equilibria. The complexes that could give rise to this behavior are shown schematically in Figure 6. The absorption band characteristic of the sandwich complex could be due to

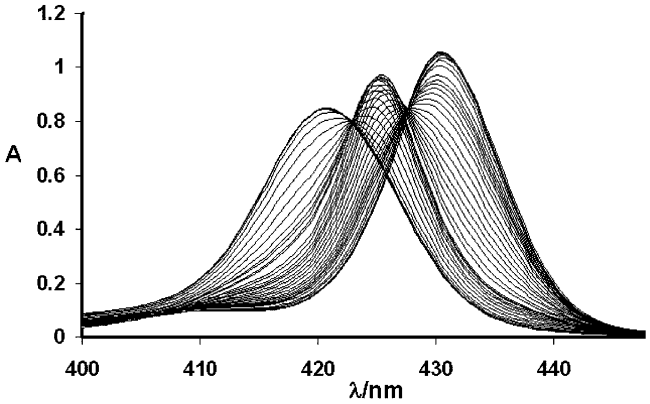

Figure 5. UV−visible titration of **9** (1 μM) with DABCO in CH_2Cl_2 at 295 K.

either intramolecular interactions in a 1:1 **9**·DABCO complex (Figure 6a) or intermolecular interactions in a 2:2 $(\mathbf{9})_2$·$(DABCO)_2$ complex (Figure 6b).

The titration data were analyzed using the program Specfit, which analyzes the whole series of spectra simultaneously.[18,19] The two different binding models shown in Figure 6 were analyzed, and both fit the titration data equally well. Figure 7 shows representative curve fits for three different wavelengths, corresponding to the λ_{max} values for the free porphyrin, the sandwich complex, and the final open complex. The fitting process optimized the extinction coefficients at each wavelength as well as the stability constants for the two complexes. The value of K_{12} provides an excellent quality control test, because it can be compared with the value of K_m previously determined for the simple monomeric model compound ($K_{12} = 4\,K_m^2$). For the intramolecular sandwich model in Figure 6a, $K_{11} = 2.6 \times 10^5$ M^{-1} and $K_{12} = 6.6 \times 10^9$ M^{-1}. This corresponds to a K_m of 4.1×10^4 M^{-1} which is close to the value measured for the monomeric model compound. For the intermolecular sandwich model in Figure 6b, $K_{22} = 6.2 \times 10^{16}$ M^{-3} and $K_{12} = 5.2 \times 10^9$ M^{-2} which corresponds to a K_m of 3.6×10^4 M^{-1}, again consistent with the value of K_m for the model compound.

The two binding models in Figure 6 cannot be distinguished from the UV−visible experiments described, but they can be differentiated by carrying out titrations at different porphyrin concentrations. The stability of the 2:2 intermolecular sandwich complex relative to free **9** and the final **9**·$(DABCO)_2$ complex depends on the concentration of porphyrin, whereas the stability of the 1:1 intramolecular sandwich complex relative to these two species is independent of porphyrin concentration. If we use the association constants determined by fitting the UV−visible titration data to predict the behavior at NMR concentrations, the two binding models look quite different (Figure 8). The 1:1 intramolecular sandwich complex is never completely formed and disappears immediately in the presence of excess DABCO at millimolar porphyrin concentrations. However, the 2:2 intermolecular sandwich complex is fully assembled at a 1:1 stoichiometry and requires a much larger concentration of DABCO for subsequent dissociation to occur.

^{1}H NMR titrations were performed by adding DABCO to a 1 mM solution of **9** in $CDCl_3$. The first additions resulted in a general broadening of the spectrum, but a new set of broad

(18) Maeder, M.; Zuberbühler, A. D. *Anal. Chem.* **1990**, *62*, 2220−2224.
(19) Gampp, H.; Maeder, M.; Meyer, C. J.; Zuberbühler, A. D. *Talanta* **1986**, *33*, 943−951.

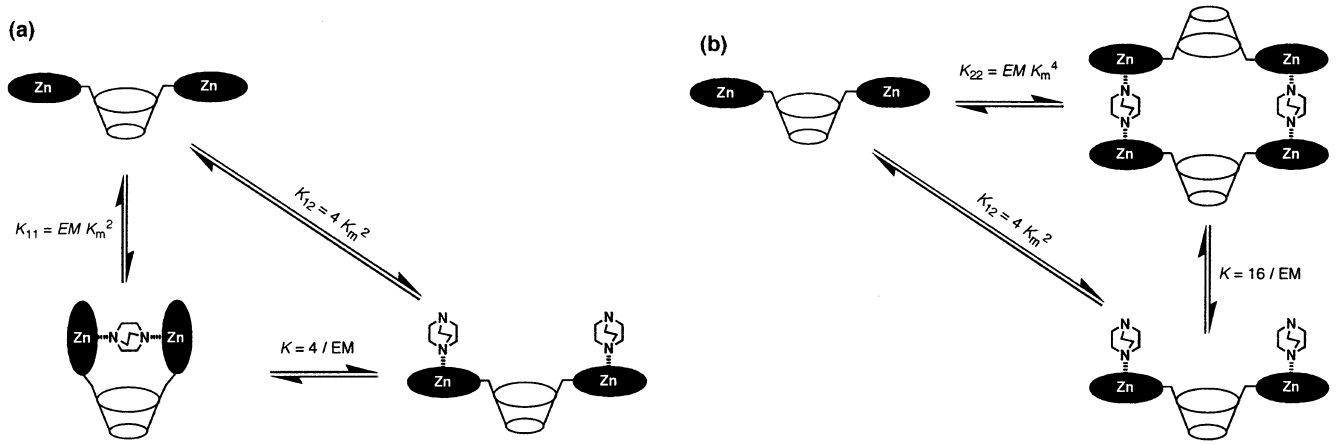

Figure 6. Possible equilibria present in mixtures of **9** and DABCO. *EM* is the effective molarity for the intramolecular interaction required for cyclization. K_m is the microscopic association constant for the interaction of one DABCO nitrogen with a zinc porphyrin. Stepwise equilibrium constants (K), overall stability constants (K_{11}, K_{22}, and K_{12}), and statistical correction factors for the equilibria are also shown.

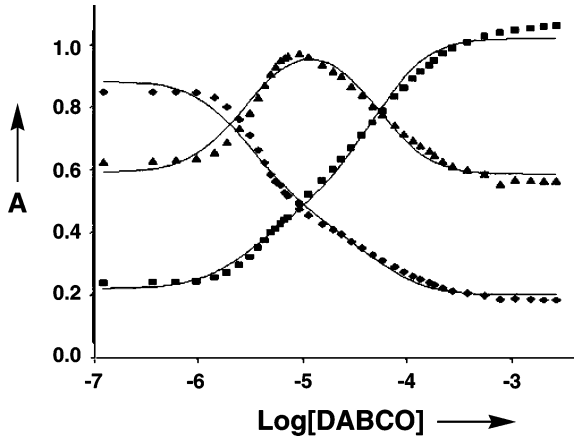

Figure 7. The UV−visible titration data for **9** (1 μM) were fit to a three-state binding model (Figure 6b). The data at 420 nm (◆), 425 nm (▲), and 430 nm (■) are shown along with the fitted curves.

signals corresponding to the sandwich complex appeared. The free and bound signals are in slow exchange on the NMR time scale. A singlet appeared at −4.7 ppm, characteristic of the DABCO protons bound in a 2:1 porphyrin−DABCO sandwich complex.[14] The 8 ppm upfield shift is due to the combined effect of the two porphyrin ring currents.[12] The bound signals due to the porphyrin β-pyrrolic protons are broad but clearly distinguishable at 8.5 ppm. The upfield shift with respect to the corresponding free porphyrin signals (−0.4 ppm) is again a consequence of the porphyrin ring current.[15] Subsequent addition of up to 1 equiv of DABCO resulted in an increase in the intensity of the bound signals and disappearance of the free signals. Only when more than 1 equiv of DABCO was added did the bound DABCO signal at −4.7 ppm broaden and disappear, as the system entered a fast exchange regime. The signals due to **9** then gradually returned to positions similar to those observed in the free state consistent with the formation of the open **9**·$(DABCO)_2$ complex. The amount of porphyrin−DABCO sandwich complex was determined by integrating the signals in the slow exchange phase of the titration, and the results match the predictions in Figure 8b rather than those in Figure 8a. This experiment shows that **9** forms the intermolecular 2:2 sandwich complex shown in Figure 6b rather than the intramolecular 1:1 complex shown in Figure 6a. Molecular models suggest that intramolecular chelation does not take place in this system, because the geometry of the calixarene spacer precludes conformations where the porphyrins are coplanar and at the correct separation to bind to the same DABCO molecule.

The value of $K_{22} = 6.2 \times 10^{16}$ M^{-3} measured in the UV−visible titration can be used to determine the effective molarity for the cyclization interaction required to form the 2:2 complex.[20,21] $K_{22} = EM\ K_m^4$, giving a value of *EM* of 0.04 M. The *EM* is the concentration at which open polymeric assemblies start to compete with the closed macrocyclic assembly.[22] Because all of the studies described here were carried out at significantly lower concentrations, no evidence of polymerization was observed. The value of *EM* is lower than some of the other self-assembled zinc porphyrin systems we have studied which can have effective molarities as high as 6 M.[22] The reduction in *EM* is probably due to small mismatches in geometry which cause strain and freezing out of some of the calixarene flexibility on complexation. Nevertheless, the four zinc−nitrogen interactions are strong enough to promote assembly of the dimeric cage shown in Figure 6b across a wide range of concentrations.

Self-Assembly of the Calix-Tetraporphyrin 1. The complexes formed between the calix-tetraporphyrin derivative **1** and DABCO were first investigated by UV−visible titration experiments. The behavior of this system is more complicated, and the results are shown in Figure 9. Initially, the porphyrin Soret band at 420 nm decreases in intensity and a new band appears at 425 nm with an isosbestic point at 423 nm characteristic of a simple two-state equilibrium. However, the titration then enters a nonisosbestic region, before a second isosbestic point appears at 428 nm, associated with an increase in intensity of a new band at 430 nm. The bands at 420, 425, and 430 nm are again characteristic of a free porphyrin, a 2:1 porphyrin−DABCO sandwich complex, and a simple 1:1 porphyrin−DABCO complex.[12] However, in this case, it appears that more than one type of sandwich complex is formed, leading to the complicated behavior in the middle part of the titration.

Because **1** has four binding sites, several different types of intramolecular or intermolecular sandwich complexes could be formed, and from the UV−visible data it is not possible to

(20) Mandolini, L. *Adv. Phys. Org. Chem.* **1986**, *22*, 1−111.
(21) Kirby, A. J. *Adv. Phys. Org. Chem.* **1980**, *17*, 183−278.
(22) Chi, X. L.; Guerin, A. J.; Haycock, R. A.; Hunter, C. A.; Sarson, L. D. *J. Chem. Soc., Chem. Commun.* **1995**, 2563−2565.

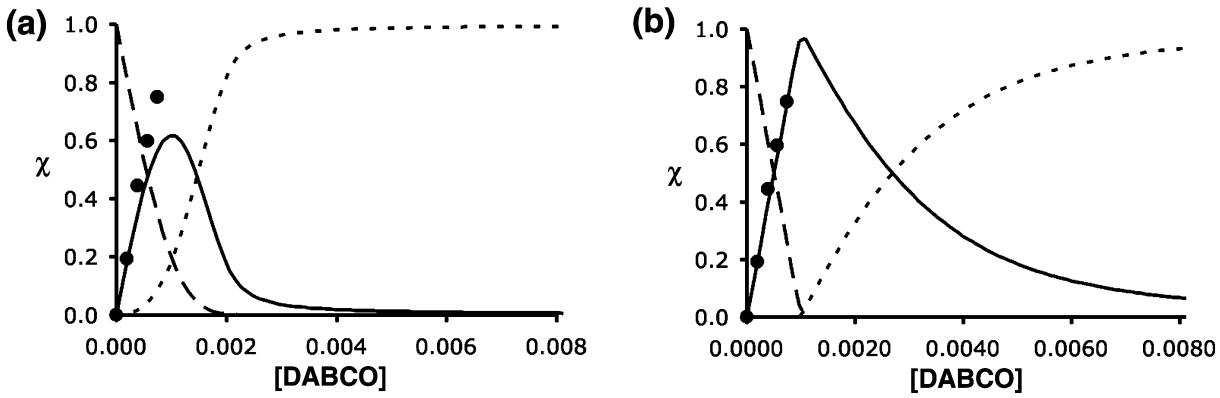

Figure 8. ^{1}H NMR titration of **9** (1 mM) with DABCO in $CDCl_3$ at 295 K. (a) Simulated concentration profiles for the intramolecular sandwich model shown in Figure 6a, showing the mole fraction of free **9** (− − −), **9**·DABCO (−), and **9**·$(DABCO)_2$ (- - -). (b) Simulated concentration profiles for the intermolecular sandwich model shown in Figure 6b, showing the mole fraction of free **9** (− − −), $(\mathbf{9})_2$·$(DABCO)_2$ (−), and **9**·$(DABCO)_2$ (- - -). The experimental mole fraction (χ) of sandwich complex (●) determined by integration of ^{1}H NMR signals in the slow exchange phase of the titration is shown for comparison.

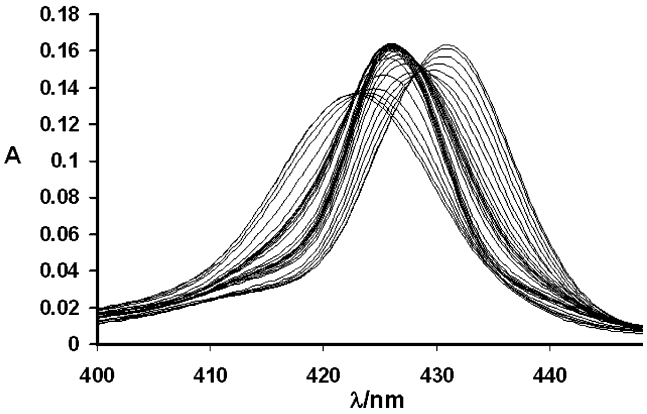

Figure 9. UV−visible titration of **1** (0.1 μM) with DABCO in CH_2Cl_2 at 295 K.

identify them. However, ^{1}H NMR spectroscopy gave further insight into the behavior of this system. When DABCO was added to a 0.5 mM solution of **1** in $CDCl_3$, the signals due to **1** broadened, and a new set of signals appeared corresponding to a DABCO complex in slow exchange with free **1**. A new signal at −4.7 ppm is indicative of DABCO sandwiched between two porphyrins in the complex.[14] Three new signals were observed for the calixarene methylene bridges and for the propyl OCH_2 protons, all of them downfield shifted with respect to free **1**. A new multiplet appeared at 8.56 ppm due to the porphyrin β-pyrrolic protons, upfield shifted by the ring current of the nearby porphyrin.

Further addition of DABCO resulted in an increase of the intensity of the new bound signals and a decrease of the signals due to free **1**. When 0.7 equiv of DABCO had been added, another new set of signals began to appear: a new bound DABCO signal around −4.7 ppm and three new signals for both the methylene calixarene bridges and the propyl OCH_2 protons, further downfield shifted. At 1 equiv of DABCO, there were three different species in slow exchange: free **1**, the sandwich complex formed initially which is the major species, and the second sandwich complex. Subsequent addition of DABCO resulted in the complete disappearance of the signals of free **1** and an increase of the intensity of the signals due to the second sandwich complex. By the time 2 equiv of DABCO had been added, the sandwich complex formed initially had disappeared and only one sandwich complex remained. On addition of more than 2 equiv of DABCO, the system entered a fast exchange regime, and all of the signals due to **1** gradually returned to positions close to those observed for free **1**. This final phase of the titration clearly reflects dissociation of the sandwich complex to give the **1**·$(DABCO)_4$ complex in the presence of excess DABCO. The two sandwich complexes have **1**:DABCO stoichiometries of 1:1 and 1:2, as is deduced by integration of the slow exchange porphyrin and DABCO signals. Figure 10a shows how the concentrations of the different species vary during the slow exchange phase of the NMR titration.

This information explains the complicated behavior in the UV−visible titration, although we cannot tell whether the sandwich complexes are intermolecular assemblies or intramolecular complexes. The UV−visible data were therefore fit to two different models using Specfit:

Model 1

$$\mathbf{1} \leftrightarrows \mathbf{1}\cdot DABCO \leftrightarrows \mathbf{1}\cdot(DABCO)_2 \leftrightarrows \mathbf{1}\cdot(DABCO)_4$$

Model 2

$$\mathbf{1} \leftrightarrows (\mathbf{1})_2\cdot(DABCO)_2 \leftrightarrows (\mathbf{1})_2\cdot(DABCO)_4 \leftrightarrows \mathbf{1}\cdot(DABCO)_4$$

In neither case was it possible to obtain a good fit to the experimental data, and it became clear that another complex must be present. If we consider Model 1, it is obvious what this species must be. The formation of an intermediate on the pathway to assembling the complex with a 1:2 **1**−DABCO stoichiometry implies that the formation of the first porphyrin−DABCO sandwich is more favorable than formation of the second. It follows that, in the presence of excess DABCO, the porphyrin−DABCO sandwiches will open up in a two-step process, generating an intermediate complex with a 1:3 **1**−DABCO stoichiometry. The titration data were therefore analyzed using models that included this additional complex:

Model 3

$$\mathbf{1} \leftrightarrows \mathbf{1}\cdot DABCO \leftrightarrows \mathbf{1}\cdot(DABCO)_2 \leftrightarrows \mathbf{1}\cdot(DABCO)_3 \leftrightarrows \mathbf{1}\cdot(DABCO)_4$$

Model 4

$$\mathbf{1} \leftrightarrows (\mathbf{1})_2\cdot(DABCO)_2 \leftrightarrows (\mathbf{1})_2\cdot(DABCO)_4 \leftrightarrows (\mathbf{1})_2\cdot(DABCO)_6 \leftrightarrows \mathbf{1}\cdot(DABCO)_4$$

Both models gave excellent fits to the experimental data. As we found for the complexes formed by **9**, the UV−visible titration data alone are insufficient to distinguish intermolecular assemblies from intramolecular complexes. However, the association constants determined from fitting the UV−visible data can be used to predict the behavior at NMR concentrations.

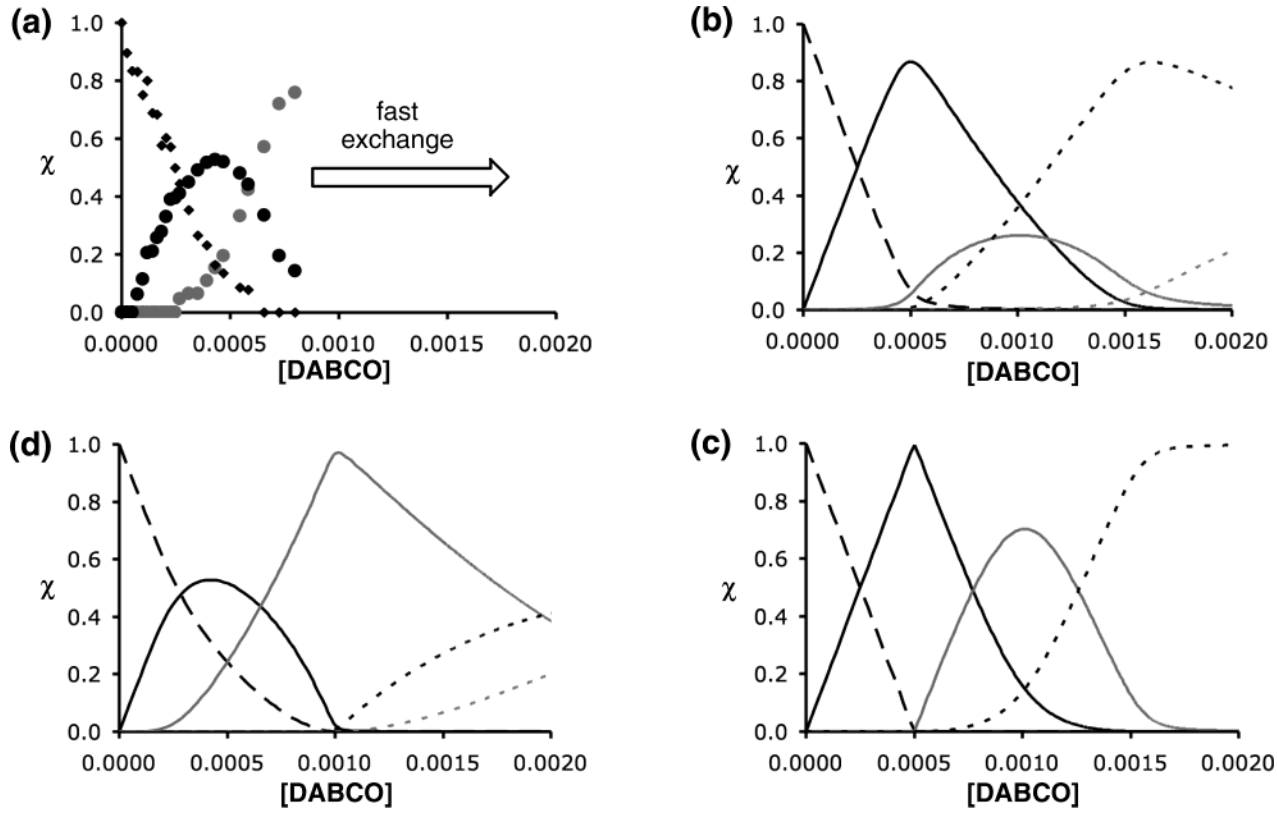

Figure 10. ^{1}H NMR titration of **1** (0.5 mM) with DABCO in $CDCl_3$ at 295 K. (a) Experimental data for the mole fraction (χ) of free **1** (◆), the 1:1 stoichiometry **1**−DABCO complex (●), and the 1:2 stoichiometry **1**−DABCO complex (gray circle). (b) Simulated concentration profiles for binding Model 3 showing the mole fraction of free **1** (− − −), **1**·DABCO (−), **1**·$(DABCO)_2$ (gray line), **1**·$(DABCO)_3$ (- - -), and **1**·$(DABCO)_4$ (gray dashed line). (c) Simulated concentration profiles for binding Model 4 showing the mole fraction of free **1** (− − −), $(\mathbf{1})_2$·$(DABCO)_2$ (−), $(\mathbf{1})_2$·$(DABCO)_4$ (gray line), $(\mathbf{1})_2$·$(DABCO)_6$ (- - -), and **1**·$(DABCO)_4$ (gray dashed line) which does not appear in this concentration range. (d) Simulated concentration profiles for binding Model 5 showing the mole fraction of free **1** (− − −), **1**·DABCO (−), $(\mathbf{1})_2$·$(DABCO)_4$ (gray line), **1**·$(DABCO)_3$ (- - -), and **1**·$(DABCO)_4$ (gray dashed line).

Models 3 and 4 give rise to quite different concentration profiles for the complexes formed with DABCO at millimolar concentrations. However, neither model predicts the experimental behavior well (compare Figure 10a with Figure 10b and c). In both cases, the first sandwich complex (1:1 or 2:2) is fully assembled at 1 equiv of DABCO, whereas, experimentally, this complex is never more than 60% populated and reaches a maximum at about 0.7 equiv of DABCO. The simplest explanation is that both intramolecular and intermolecular sandwich complexes are formed, and Model 5 below gave an excellent fit to both the UV−visible data (Figure 11) and the slow exchange phase of the NMR titration (Figure 10d). Figure 12 illustrates the structures of the different species involved.

Model 5

$$\mathbf{1} \leftrightarrows \mathbf{1}\cdot DABCO \leftrightarrows (\mathbf{1})_2\cdot(DABCO)_4 \leftrightarrows \mathbf{1}\cdot(DABCO)_3 \leftrightarrows \mathbf{1}\cdot(DABCO)_4$$

The equilibrium constants extracted from the Specfit procedure provide further insight into the structures of the **1**−DABCO complexes. The value of $K_{14} = 7.6 \times 10^{19}$ M^{-4} corresponds to a K_m of 4.7×10^4 M^{-1} which is identical to the value obtained for **9** and very close to the value of K_m measured for the monomeric model compound, providing confidence in the quality of the fit to the experimental data. The other association constants are $K_{11} = 2.0 \times 10^7$ M^{-1}, $K_{24} = 6.3 \times 10^{33}$ M^{-5}, and $K_{13} = 3.2 \times 10^{17}$ M^{-3}. From the experiments with the calix-bisporphyrin **9**, we know that the stability of the intramolecular sandwich complex that could be formed between two diametral

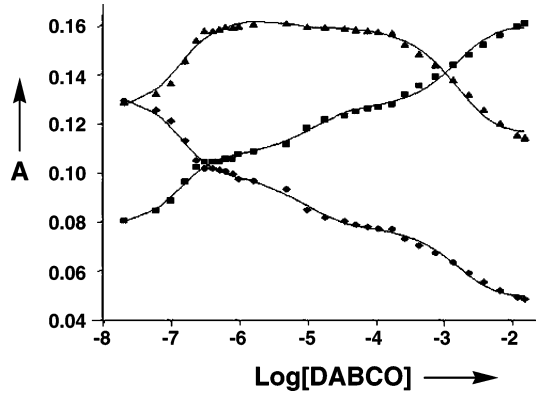

Figure 11. The UV−visible titration data for **1** with DABCO were fit to the four-state binding Model 5. The data at 420 nm (◆), 425 nm (▲), and 430 nm (■) are shown along with the fitted curves.

(1,3) porphyrins must be less than the apparent value of K_{11} for this system, 2.6×10^5 M^{-1}. The 1:1 complex formed by **1** and DABCO is 2 orders of magnitude more stable and must therefore involve two proximal (1,2) porphyrins. Figure 12 shows the structures of all of the species present in mixtures of **1** and DABCO. The values of K_{11} and K_{13} allow us to make two independent estimates of EM_1, the effective molarity for the intramolecular interaction to form a DABCO sandwich complex between the two proximal (1,2) porphyrins. The values of EM_1 obtained using the equations in Figure 12 are 0.002 and 0.004 M using the values of K_{11} and K_{13}, respectively. The excellent agreement provides another indication of the quality

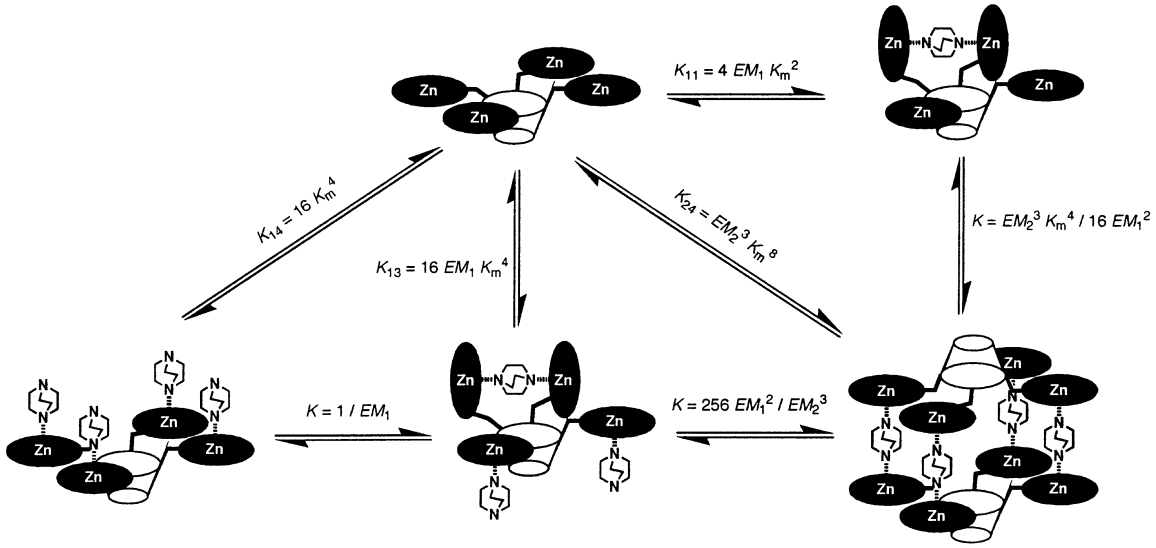

Figure 12. Equilibria present in mixtures of **1** and DABCO. EM_1 and EM_2 are the effective molarities for the intramolecular interactions required to form the intramolecular and intermolecular sandwich complexes 1·DABCO and $(\mathbf{1})_2$·$(DABCO)_4$, respectively. K_m is the microscopic association constant for the interaction of one DABCO nitrogen with a zinc porphyrin. Stepwise equilibrium constants (K), overall stability constants (K_{11}, K_{24}, K_{13}, and K_{14}), and statistical correction factors for the equilibria are also shown.

of the fitting process. If we assume that the effective molarity for each intramolecular interaction required to assemble the 2:4 cage complex is identical, we can use the value of K_{24} to estimate $EM_2 = 0.06$ M (Figure 12). This effective molarity is in good agreement with the value determined for formation of the intermolecular sandwich complex with compound **9** (0.04 M). It appears that formation of the 1:1 complex causes a significant distortion of the calixarene scaffold, as is evidenced by the changes in the ^{1}H NMR signals due to the calixarene protons, and this conformational change precludes binding of a second molecule of DABCO in an intramolecular fashion. Thus, the second DABCO binding interaction causes the 1:1 complex to open up to the 2:4 sandwich, allowing all coordination sites to be simultaneously satisfied.

Conclusions

In summary, we have shown that it is possible to achieve the self-assembly of calixarene capsules through metalloporphyrin−ligand coordination. The calix-bisporphyrin **9** forms a simple 2:2 complex with DABCO, but the calix-tetraporphyrin **1** shows remarkable flexibility in the range of DABCO complexes that it forms. Initially, an intramolecular 1:1 complex is formed, but this opens up to yield the 2:4 cage complex in the presence of more DABCO. When excess DABCO is added, the cage collapses to the simple 1:4 complex in a two-step process via a 1:3 complex which contains an intramolecular DABCO sandwich. These complicated equilibria were characterizable in this system, because we were able to study the complexation in detail using both UV−visible and ^{1}H NMR spectroscopy. Using a single concentration range, it is impossible to tell whether titration data are best described by a simple complexation event or by a higher order self-assembly process. The reason is that the binding isotherms for these processes are indistinguishable, unless the titrations are carried out over a much wider concentration range. If we compare the micromolar regime used for UV−visible experiments with the millimolar regime used for ^{1}H NMR experiments, then simple complexation and higher order self-assembly processes can easily be distinguished, because they lead to quite different behavior. The stability of higher order assemblies increases significantly with concentration, whereas simple complexes are much less sensitive to concentration. The cage complexes described here feature large well-defined cavities, and their potential as supramolecular hosts is currently under investigation.

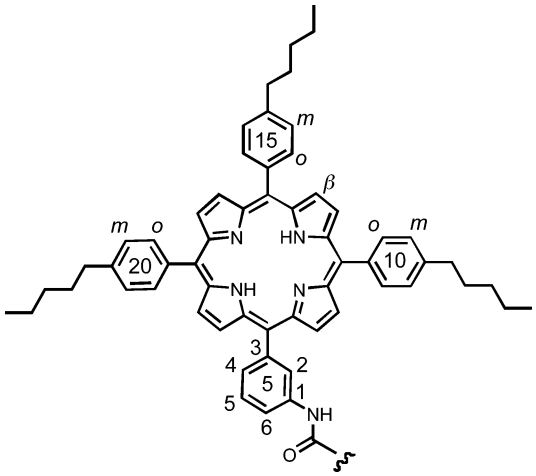

Figure 13. The porphyrin numbering scheme used to assign the NMR data.

Experimental Section

Titrations. ^{1}H NMR and UV−visible titrations were performed by adding solutions of DABCO to a solution of the calixarene in either a 5 mm NMR tube or a 1 cm path length quartz cuvette using microliter syringes (Figure 13). In the UV−visible titrations, the calixarene was present in the guest solution at the same concentration as that in the cuvette to avoid dilution effects. UV−visible titrations were analyzed by fitting the whole series of spectra at 0.5 nm intervals using the software Specfit version 3.0.22 (from Spectrum Software Associates, P.O. Box 4494, Chapel Hill, NC 27515-4494), which uses a global analysis system with expanded factor analysis and Marquardt least-squares minimization to obtain globally optimized parameters.[18,19]

Synthesis. Free Base Calix-Tetraporphyrin 5. To a suspension of calixarene **2** (38 mg, 0.05 mmol) in dry CH_2Cl_2 (10 mL) was added

oxalyl chloride (0.26 mL, 3 mmol). The mixture was refluxed under nitrogen until the solid was completely dissolved (48 h) and evaporated to dryness to give **3** as an oil. Without any further purification, the crude product was dissolved in dry CH_2Cl_2 (5 mL) and added dropwise to a solution of porphyrin **4** (0.5 g, 0.6 mmol) in dry CH_2Cl_2 (50 mL). After being stirred for 3 h under nitrogen, the reaction was quenched with H_2O (30 mL) and extracted with CH_2Cl_2 (20 mL). The organic layer was washed with saturated $NaHCO_3$, dried over Na_2SO_4, and the solvent was evaporated under reduced pressure. The product was separated from the unreacted porphyrin by flash chromatography on silica gel eluting first with CH_2Cl_2−hexane (1:1) to recover the porphyrin **4** and then with CH_2Cl_2−CH_3OH (100:1) to yield pure **5** as a purple powder (85 mg, 42%): mp 243−244 °C. ^{1}H NMR ($CDCl_3$, 300 MHz): δ 8.82 (d, 8H, J = 4.8 Hz, β-pyrrolic H), 8.70 (d, 8H, J = 4.8 Hz, β-pyrrolic H), 8.69 (d, 8H, J = 4.8 Hz, β-pyrrolic H), 8.62 (d, 8H, J = 4.8 Hz, β-pyrrolic H), 8.32 (s, 8H, CONH and 5-H_2), 8.08 (d, 4H, J = 7.0 Hz, 15-H_o), 7.95 (d, 4H, J = 6.9 Hz, 15-H_o), 7.82 (d, 8H, J = 7.0 Hz, 10- and 20-H_o), 7.76 (m, 12H, 10- and 20-H_o and 5-H_6), 7.51 (d, 4H, J = 7.0 Hz, 15-H_m), 7.40 (d, 4H, J = 6.9 Hz, 15-H_m), 7.34 (s, 8H, ArH), 7.35 (d, 4H, J = 7.8 Hz, 5-H_4), 7.19 (d, 8H, J = 7.0 Hz, 10- and 20-H_m), 6.96 (d, 8H, J = 7.2 Hz, 10- and 20-H_m), 6.66 (t, 4H, J = 7.8 Hz, 5-H_2), 4.51 (d, 4H, J = 13.8 Hz, $ArCH_2Ar$), 3.89 (t, 8H, J = 7.2 Hz, CH_2), 3.31 (d, 4H, J = 13.8 Hz, $ArCH_2Ar$), 2.90 (t, 8H, J = 7.5 Hz, CH_2), 2.57 (t, 16H, J = 7.5 Hz, CH_2), 1.87 (m, 16H, CH_2), 1.60 (m, 16H, CH_2), 1.51 (m, 16H, CH_2), 1.27 (m, 32H, CH_2), 1.00 (t, 12H, J = 6.9 Hz, CH_3), 0.95 (t, 12H, J = 7.5 Hz, CH_3), 0.85 (t, 24H, J = 7.0 Hz, CH_3), −2.77 (s, 8H, NH). ^{13}C NMR ($CDCl_3$, 75 MHz): δ 166.2 (s, CO), 159.4 (s, Ar_i), 142.5 (s, α-pyrrolic C), 142.1 (s, 15-C_i), 141.8 (s, 10- and 20-C_i), 139.4 (s, 15-C_p), 139.1 (s, 10- and 20-C_p), 136.3 (s, 5-C_1), 135.0 (s, 5-C_3), 134.4 (d, 10-, 15-, and 20-C_o), 134.3 (d, 10-, 15-, and 20-C_o), 131.0 (bs, β-pyrrolic C), 130.6 (d, 5-C_4), 129.7 (s, Ar_o), 127.6 (d, Ar_m), 126.8 (d, 5-C_5), 126.5 (d, 10-, 15-, and 20-C_m), 126.3 (2d, 10-, 15-, and 20-C_p and 5-C_2), 120.0 (s, *meso*-porphyrinic C), 119.6 (d, 5-C_6), 119.1 (s, Ar_p), 77.1 (t, CH_2), 35.9 (t, CH_2), 35.6 (t, CH_2), 31.7 (t, CH_2), 31.5 (t, CH_2), 31.3 (t, CH_2), 31.0 (t, CH_2), 29.6 (t, $ArCH_2Ar$), 23.1 (t, CH_2), 22.6 (t, CH_2), 22.5 (t, CH_2), 14.1 (q, CH_3), 14.0 (q, CH_3), 10.1 (q, CH_3). UV−vis (CH_2Cl_2): λ_{max}/nm 420, 515, 551, 590, 647. *m*/*z* (MALDI-TOF) 4055.4 (M + 1, $C_{280}H_{284}N_{20}O_8$ requires 4054.24).

Zinc Calix-Tetraporphyrin 1. 5 (80 mg, 0.02 mmol) was dissolved in CH_2Cl_2 (30 mL), and a solution of zinc acetate (146 mg, 0.8 mmol) in CH_3OH (10 mL) was added. The reaction mixture was stirred at room temperature for 5 h, filtered through basic alumina, and evaporated to dryness. Recrystallization from CH_2Cl_2−CH_3OH yielded pure **1** as a purple powder (82 mg, 95%): mp 255−258 °C. ^{1}H NMR ($CDCl_3$, 300 MHz): δ 8.81 (m, 32H, β-pyrrolic H), 8.30 (s, 4H, 5-H_2), 8.26 (s, 4H, CONH), 8.07 (d, 4H, J = 7.2 Hz, 15-H_o), 7.98 (d, 4H, J = 7.2 Hz, 15-H_o), 7.96 (d, 8H, J = 7.2 Hz, 10- and 20-H_o), 7.86 (m, 12H, 10- and 20-H_o and 5-H_6), 7.58 (d, 4H, J = 7.5 Hz, 5-H_4), 7.49 (d, 4H, J = 7.2 Hz, 15-H_m), 7.43 (d, 4H, J = 7.2 Hz, 15-H_m), 7.33 (m, 16H, ArH and 10- and 20-H_m), 7.13 (d, 8H, J = 7.2 Hz, 10- and 20-H_m), 7.03 (t, 4H, J = 7.5 Hz, 5-H_2), 4.51 (d, 4H, J = 13.6 Hz, $ArCH_2Ar$), 3.89 (t, 8H, J = 7.0 Hz, CH_2), 3.31 (d, 4H, J = 13.6 Hz, $ArCH_2Ar$), 2.91 (t, 8H, J = 7.3 Hz, CH_2), 2.67 (t, 16H, J = 7.5 Hz, CH_2), 1.90 (m, 16H, CH_2), 1.63 (m, 16H, CH_2), 1.51 (m, 16H, CH_2), 1.33 (m, 32H, CH_2), 1.00 (t, 12H, J = 6.9 Hz, CH_3), 0.94 (t, 12H, J = 7.5 Hz, CH_3), 0.88 (t, 24H, J = 6.9 Hz, CH_3). UV−vis (CH_2Cl_2): λ_{max}/nm (ϵ/dm^3 mol^{-1} cm^{-1}) 421 (1 340 000), 549 (86 000), 588 (27 000). *m*/*z* (MALDI-TOF) 4302.8 (M + 1, $C_{280}H_{276}N_{20}O_8Zn_4$ requires 4301.90).

Free Base Calix-Bisporphyrin 8. To a suspension of calixarene **6** (30 mg, 0.044 mmol) in dry CH_2Cl_2 (10 mL) was added oxalyl chloride (0.12 mL, 1.32 mmol). The mixture was refluxed under nitrogen until the solid was completely dissolved (24 h) and evaporated to dryness to give **7** as an oil. Without any further purification, the crude product was dissolved in dry CH_2Cl_2 (5 mL) and added dropwise to a solution of porphyrin **4** (0.22 g, 0.26 mmol) in dry CH_2Cl_2 (30 mL). After being stirred for 3 h under nitrogen, the reaction was quenched with H_2O (30 mL) and extracted with CH_2Cl_2 (20 mL). The organic layer was washed with saturated $NaHCO_3$, dried over Na_2SO_4, and the solvent was evaporated under reduced pressure. The product was separated from the unreacted porphyrin by flash chromatography on silica gel eluting first with CH_2Cl_2−hexane (1:1) to recover the porphyrin **4** and then with CH_2Cl_2−CH_3OH (50:1) to yield pure **8** as a purple powder (46 mg, 45%). ^{1}H NMR ($CDCl_3$, 400 MHz): δ 8.86 (d, 4H, J = 4.8 Hz, β-pyrrolic H), 8.84 (d, 4H, J = 4.8 Hz, β-pyrrolic H), 8.79 (d, 4H, J = 4.8 Hz, β-pyrrolic H), 8.73 (d, 4H, J = 4.8 Hz, β-pyrrolic H), 8.31 (s, 2H, 5-H_2), 8.11 (d, 2H, J = 7.6 Hz, 5-H_6), 8.10 (d, 4H, J = 6.6 Hz, 15-H_o), 7.99 (s, 2H, CONH), 7.96 (d, 4H, J = 7.6 Hz, 10- and 20-H_o), 7.86 (d, 4H, J = 7.6 Hz, 10- and 20-H_o), 7.69 (d, 2H, J = 7.6 Hz, 5-H_4), 7.54 (d, 4H, J = 6.6 Hz, 15-H_m), 7.37 (t, 2H, J = 7.6 Hz, 5-H_5), 7.36 (d, 4H, J = 7.6 Hz, 10- and 20-H_m), 7.25 (s, 4H, ArH), 7.20 (d, 4H, J = 7.6 Hz, 10- and 20-H_m), 6.64 (d, 4H, J = 7.4 Hz, ArH), 6.54 (t, 2H, J = 7.4 Hz, ArH), 4.46 (d, 4H, J = 13.2 Hz, $ArCH_2$-Ar), 3.86 and 3.85 (2t, 4H each, J = 7.0 Hz, CH_2), 3.21 (d, 4H, J = 13.2 Hz, $ArCH_2Ar$), 2.94 (t, 4H, J = 7.5 Hz, CH_2), 2.76 (t, 8H, J = 7.5 Hz, CH_2), 1.90 (m, 12H, CH_2), 1.77 (m, 8H, CH_2), 1.53 (m, 8H, CH_2), 1.45 (m, 16H, CH_2), 1.02 (t, 6H, J = 7.0 Hz, CH_3), 0.96 (m, 20H, CH_3), −2.77 (s, 4H, NH). ^{13}C NMR ($CDCl_3$, 62.5 MHz): δ 166.5 (s, CO), 159.6 (s, Ar_i), 156.5 (s, Ar_i), 142.6 (s, α-pyrrolic C), 142.3 (s, 15-C_i), 142.0 (s, 10- and 20- C_i), 139.5 (s, 15-C_p), 139.3 (s, 10- and 20- C_p), 136.7 (s, 5-C_1), 135.3 (s, 5-C_3), 134.8 (s, Ar_o), 134.6 (d, 10-, 15-, and 20-C_o), 134.4 (d, 10-, 15-, and 20-C_o), 131.0 (bs, β-pyrrolic C), 128.8 (s, Ar_o), 128.7 (d, 5-C_4), 127.2 (d, Ar_m), 127.0 (d, Ar_m), 126.6 (2d, 10-, 15-, and 20-C_m and 5-C_5), 126.4 (2d, 10-, 15-, and 20-C_m and 5-C_2), 122.6 (d, Ar_p), 120.2 (d, 5-C_5), 120.1 (s, *meso*-porphyrinic C), 119.3 (s, Ar_p), 76.9 (t, CH_2), 35.9 (t, CH_2), 35.7 (t, CH_2), 31.8 (t, CH_2), 31.7 (t, CH_2), 31.3 (t, CH_2), 31.1 (2t, CH_2 and $ArCH_2Ar$), 23.3 (t, CH_2), 23.1 (t, CH_2), 22.7 (t, CH_2), 22.6 (t, CH_2), 14.1 (q, CH_3), 10.4 (q, CH_3), 10.1 (q, CH_3). UV−vis (CH_2Cl_2): λ_{max}/nm 420, 517, 552.5, 592, 648. *m*/*z* (MALDI-TOF) 2324.0 (M + 1, $C_{160}H_{166}N_{10}O_6$ requires 2323.30).

Zinc Calix-Bisporphyrin 9. 8 (30 mg, 0.013 mmol) was dissolved in CH_2Cl_2 (15 mL), and a solution of zinc acetate (47 mg, 0.26 mmol) in CH_3OH (5 mL) was added. The reaction mixture was stirred at room temperature for 4 h, filtered through basic alumina, and evaporated to dryness. Recrystallization from CH_2Cl_2−CH_3OH yielded pure **9** as a purple powder (31 mg, 97%): mp 231−233 °C. ^{1}H NMR ($CDCl_3$, 250 MHz): δ 8.94 (m, 14H, β-pyrrolic H and CONH), 8.84 (d, 4H, J = 4.6 Hz, β-pyrrolic H), 8.26 (s, 2H, 5-H_2), 8.11 (d, 2H, J = 7.6 Hz, 5-H_6), 8.09 (d, 4H, J = 6.6 Hz, 15-H_o), 7.97 (d, 4H, J = 7.6 Hz, 10- and 20-H_o), 7.92 (d, 4H, J = 7.6 Hz, 10- and 20-H_o), 7.80 (d, 2H, J = 7.6 Hz, 5-H_4), 7.53 (d, 4H, J = 6.6 Hz, 15-H_m), 7.46 (t, 2H, J = 7.6 Hz, 5-H_5), 7.37 (d, 4H, J = 7.6 Hz, 10- and 20-H_m), 7.26 (d, 4H, J = 7.6 Hz, 10- and 20-H_m), 7.19 (s, 4H, ArH), 6.50 (m, 6H, ArH), 4.41 (d, 4H, J = 14.0 Hz, $ArCH_2Ar$), 3.81 and 3.79 (2t, 4H each, J = 7.1 Hz, CH_2), 3.14 (d, 4H, J = 14.0 Hz, $ArCH_2Ar$), 2.95 (t, 4H, J = 7.6 Hz, CH_2), 2.78 (t, 8H, J = 7.4 Hz, CH_2), 1.85 (m, 20H, CH_2), 1.53 (m, 24H, CH_2), 0.93 (m, 30H, CH_3). UV−vis (CH_2Cl_2): λ_{max}/nm (ϵ/dm^3 mol^{-1} cm^{-1}) 420.5 (845 000), 549 (42 800), 587.5 (10 500). *m*/*z* (MALDI-TOF) 2448.5 (M + 1, $C_{160}H_{162}N_{10}O_6Zn_2$ requires 2447.13).

Acknowledgment. We thank the British Council, DGI of the Ministerio de Ciencia y Tecnología Spain (Project BQU-2002-04651), and FIRB (Project RBNE019H9K Manipolazione molecolare per macchine nanometriche) for financial support.

JA036758A